Progress In Electromagnetics Research M, Vol. 75, 179–191, 2018

Effects of Defected Waveguide Structure toward Wideband Monopole Antennas

Shu J. Chin*, Mohamad Z. A. Abd. Aziz, Mohd R. Ahmad, and Mohd A. Othman

Abstract—This paper presented the effects of Defected Waveguide Structure (DWS) toward wideband monopole antennas. Ultra-wideband (UWB) technology was introduced to support high data rate and maximum bandwidth utilization. Monopole antenna received great attention owing to its appealing features of planar in the structure and is easy to manufacture in miniaturized sizes. Yet, poor gain and directivity are always the drawbacks of the miniaturized antennas. It was found that there was no research work done on the monopole antenna design with DWS. Two wideband monopole antennas with a microstrip feed line and coplanar waveguide (CPW) feed line were proposed. Two waveguides with full copper and square DWS were designed at all the inner walls. Monopole antennas were then integrated in the waveguides. The antenna parameters studied were return loss, efficiency, gain, directivity and radiation pattern to investigate the effects of DWS toward monopole antennas. Both monopole antennas achieved wide bandwidth from 2.5 GHz to 11 GHz and higher efficiency of more than −2 dB. Monopole antennas with waveguide presented a narrower bandwidth from 6 GHz to 11 GHz but a significant directivity improvement of 5 dBi at a lower frequency of 4.5 GHz. Monopole antenna with square DWS demonstrated high directivity and gain in a wide bandwidth of 8.5 GHz. Higher gain was improved around 4 dB at the frequency of 4.5 GHz, and high efficiency of more than −2 dB was achieved. The DWS design served as a guide for future communication system based on the smart technology system.

1. INTRODUCTION

In recent years, a burgeoning demand on high resolution and high data rate has kept growing in the modern communication technology. Thus, ultra-wideband (UWB) technology was developed to support maximum bandwidth. This had made the wideband antennas become essential in a system to support the requirements [1–5]. Monopole antenna has been one of the focuses of interest for its low profile and low cost compared to other wideband antennas [6]. Yet, monopole antenna showed poor gain and directivity with low profile. Several methods have been proposed to improve the monopole antenna gain with techniques designing the radiate element in the array configuration [7] or by placing Frequency Selective Surface (FSS) [8], Artificial Magnetic Conductor (AMC) [9] underneath the antenna as a reflector. The radiating patch designed in the array configuration changed the monopole antenna design to become complex. Meanwhile, the utilization of reflector as an external design avoided the reconfiguration of monopole antenna. However, it was bulky in size as higher gain required a larger dimension of reflector.

Meanwhile, research works on the waveguide have been covered extensively over the years, and a keen interest in its applications such as filter and antenna [10–13] is evolving. In [11], the rectangular waveguide antenna with dual-polarizations worked at 9 GHz frequency for a weather radar application. Meanwhile, the waveguide filter designed in [13] worked as a bandpass filter at 72.2 GHz–73.8 GHz with

Received 14 June 2018, Accepted 6 September 2018, Scheduled 13 November 2018

* Corresponding author: Shu Jia Chin (shujia2605@gmail.com).

The authors are with the Center for Telecommunication Research and Innovation (CeTRI), Fakulti Kejuruteraan Elektronik & Kejuruteraan Komputer (FKEKK), Universiti Teknikal Malaysia Melaka (UTeM), Hang Tuah Jaya, Durian Tunggal, Melaka 76100, Malaysia.

an E-plane inserted metal strip. In addition, there were also a few researchers that designed waveguides with metamaterial [14, 15]. In [14], an H-shaped conductor partition was loaded in a proposed waveguide to pose a left-handed nature, whereas the waveguide in [15] was reconfigured by an electromagnetic bandgap (EBG) surface to cover the side walls of the waveguide. The reflection and transmission through this waveguide have been studied.

Metamaterial is also one of the hot topics discussed among researchers. It achieves negative permittivity and permeability at the same time [16]. Examples of types of metamaterial are EBG, FSS, Defected Ground Structure (DGS) and Defected Microstrip Structure (DMS) [17–20]. Defected structure is defined as a structure proposed to remove some parts of the copper layer in any shape. For instance, DMS in [20] was created at a microstrip feed line multiband antenna with tapper techniques and slot method to enhance the bandwidth. DGS in [21] was designed in a rotated "8" slot at the ground plane for a monopole antenna to enhance the bandwidth. As mentioned earlier, defected structure was applied at the ground plane and microstrip feed line as DGS and DMS, respectively. Yet, the Defected Waveguide Structure (DWS) design was not proposed. The motivation of this paper was to design a DWS with monopole antennas.

In this paper, two monopole antennas were designed with DWS externally at a frequency range of 3.1 GHz–10.6 GHz. The monopole antennas were integrated in a waveguide with full copper and DWS. The simple square DWS was presented in this paper. The performances of DWS toward monopole antennas were investigated through antenna parameters.

2. METHODS AND MATERIALS

Two circular patches of monopole antennas were designed in a microstrip feed line and CPW feed line [22–24]. A microstrip-fed monopole antenna was named Design A and composed of front and back copper layers in between an FR4 substrate as presented in Figure 1(a). Meanwhile, a CPW-fed monopole antenna was named Design B and composed of only single copper layer in front of the FR4 substrate as illustrated in Figure 1(b).

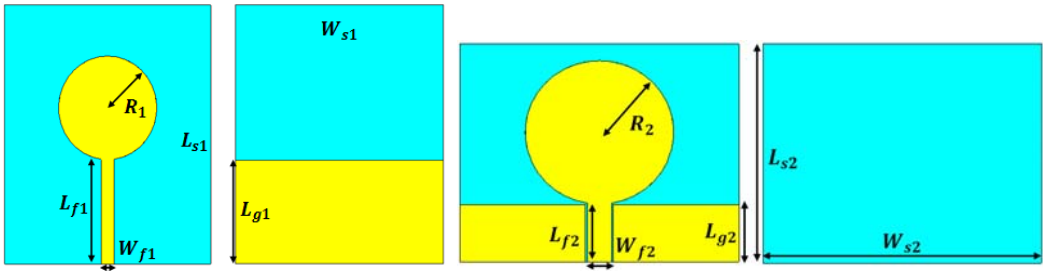

Figure 1. The front and back view of (a) Design A and (b) Design B.

The material of FR4 substrate showed a dielectric constant of 4.4, tangent loss of 0.019 and thickness of 1.6 mm while the copper presented a thickness of 0.035 mm. W_S and L_S represented the width and height of the substrate. In the meantime, the width and height of feed line were labeled as W_f and L_f, respectively. The height of the ground plane was labeled as L_g, whereas the radius of the circular radiating patch was labeled as R. The design structures of Design A and Design B with antenna parameters are shown in Figure 1 and Table 1. For design reference purposes, equations for the circular patch, microstrip feed line and CPW feed line were calculated to operate for the wideband applications [25, 26].

Monopole antennas were integrated in the waveguide with full copper at all the walls (Design C). Waveguide was designed with two different aperture dimensions of the two monopole antennas. It is known that the aperture dimension with width × height ($a \times b$) defined the cutoff frequency (f_c) [10]. The larger a and b attained a higher f_c. The f_c calculated for both the designs was around 3 GHz–3.4 GHz. Moreover, there was a limitation circumstance for the waveguide length (L_w). L_w was required

Table 1. Antenna parameters and values.

Antenna Parameters of Design A	Values	Antenna Parameters of Design B	Values
R_1	10 mm	R_2	12.5 mm
L_{S1}	50 mm	L_{S2}	38 mm
W_{S1}	42 mm	W_{S2}	47 mm
L_{f1}	20.3 mm	L_{f2}	10.3 mm
W_{f1}	2.6 mm	W_{f2}	4 mm
L_{g1}	20 mm	L_{g2}	10 mm

to achieve the minimum length of one full wave cycle of the longest wavelength; for this case, around 100 mm at 3 GHz. L_w was determined by the periodic of square DWS element with a gap which was closest to the longest wavelength. Thus, L_w was fixed at 120 mm. Design A and Design B that were designed with waveguides were simply labeled as Design AC and Design BC respectively as presented in Figure 2. Table 2 shows the antenna parameters and their values for Design AC and Design BC.

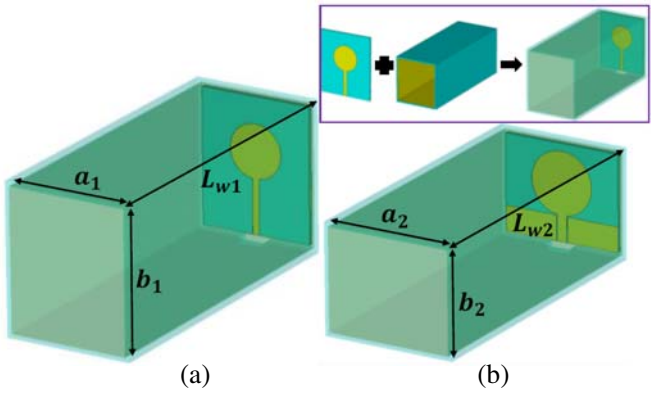

Figure 2. The perspective view of (a) Design AC and (b) Design BC.

Table 2. Antenna parameters and values.

Antenna Parameters of Design AC	Values	Antenna Parameters of Design BC	Values
a_1	44 mm	a_2	49 mm
b_1	52 mm	b_2	40 mm
L_{w1}	120 mm	L_{w2}	120 mm

On the other hand, the waveguides with DWS retained a similar dimension and length of the previous waveguide. A periodic square DWS was designed at the inner walls of the waveguide by eliminating some portions of copper layer. The square DWS was designed to cover all the inner walls in maximum number. Hence, the total number of square DWS element was not similar based on the different dimensions of the waveguide walls. The optimized square dimension (W_{sq}) and inter space square DWS (G_{sq}) were obtained through parameter studies as presented in the Results part. Figure 3 shows the optimized square DWS with the values in Table 3. The overall design structures of Design AD and Design BD are displayed in Figure 4. All the fabricated prototypes are shown in Figure 5.

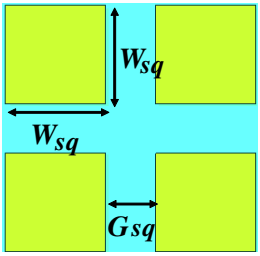

Figure 3. Unit square DWS.

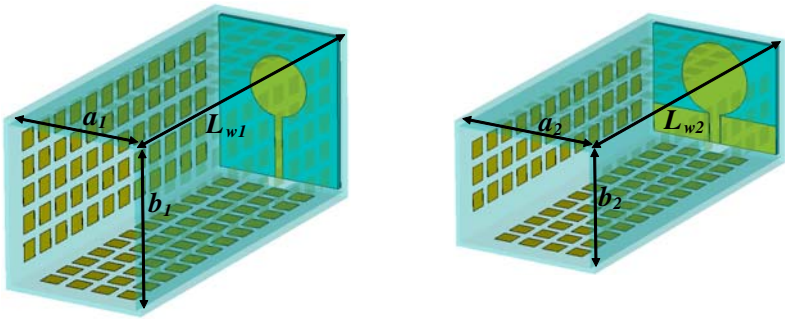

Figure 4. The perspective view of (a) Design AD and (b) Design BD.

Table 3. Antenna parameters and values.

Antenna Parameters	Values
W_{sq}	6 mm
G_{sq}	3 mm

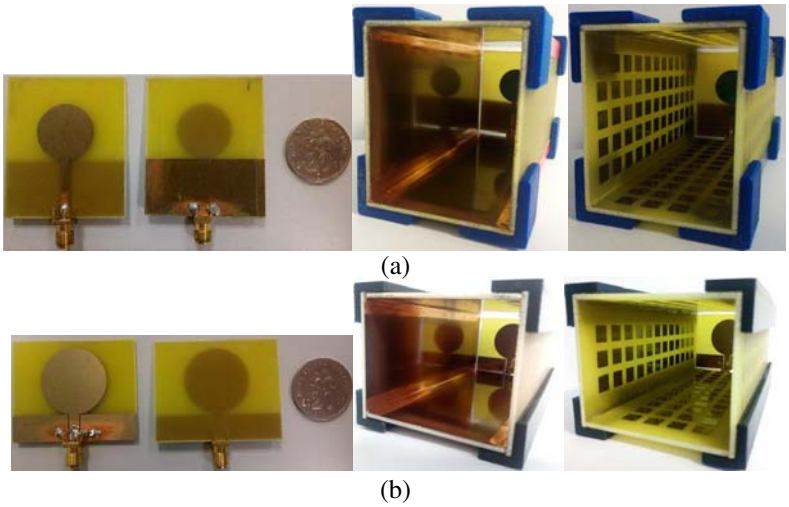

Figure 5. The fabricated prototype of (a) Design A, Design AC, Design AD and (b) Design B, Design BC, Design BD.

3. RESULTS

3.1. Effect of Square DWS Dimension (W_{sq})

A study of W_{sq} was carried out from 3.6 mm to 10.8 mm as presented in Figure 6. With the increment of W_{sq}, higher reflection and lower transmission were achieved at higher frequencies. When W_{sq} was increased, the cycle S_{11} appeared narrower with small magnitude of ripples at higher frequency range. Meanwhile, S_{21} also varied substantially with lower transmission at higher frequency, and thus the operating bandwidth was reduced. The lowest S_{21} point (in solid circle) after the operating bandwidth (S_{21} below -10 dB) was shifted to the lower frequency from Marker 1 at 9.98 GHz to Marker 3 at 5.71 GHz. The larger W_{sq} of 8.4 mm and 10.8 mm created another lower S_{21} (in dashed circle) above 9 GHz. The smallest W_{sq} of 3.6 mm performed an almost high pass along the simulated frequencies with lower reflection. Although W_{sq} of 3.6 mm presented a passband throughout the simulated frequencies, it was too small to be modified and replaced by other shapes. Hence, W_{sq} of 6 mm was chosen with the operating bandwidth B_{w1} from 3 GHz to 7.6 GHz.

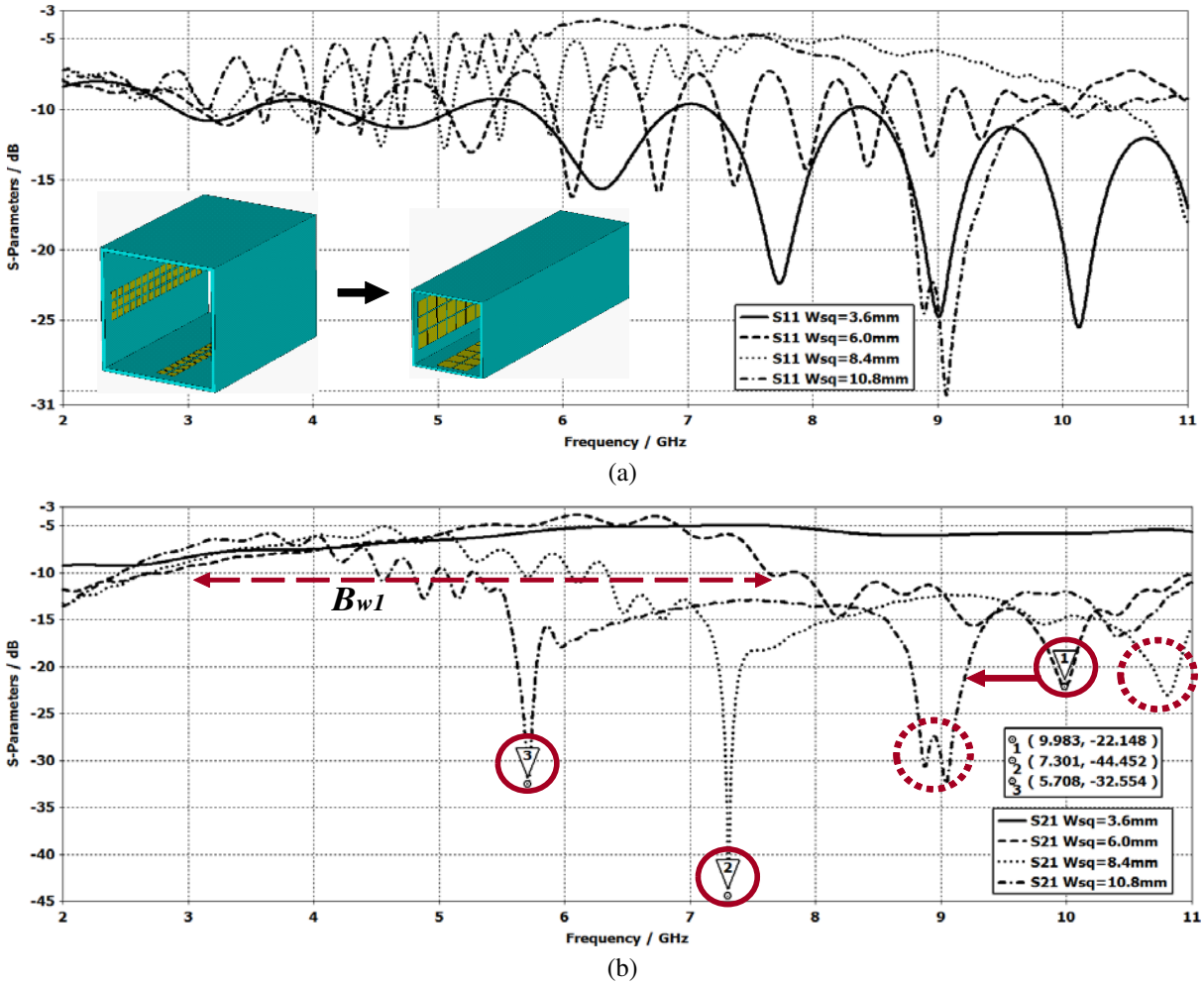

Figure 6. Simulated (a) S_{11} and (b) S_{21} for the parameter study on the square DWS dimension.

3.2. Effect of Inter Space Square DWS (G_{sq})

G_{sq} was also studied as depicted in Figure 7. Compared to the study on dimension, the study on G_{sq} from 1 mm to 7 mm demonstrated less significant alteration on the S-parameters result. It was

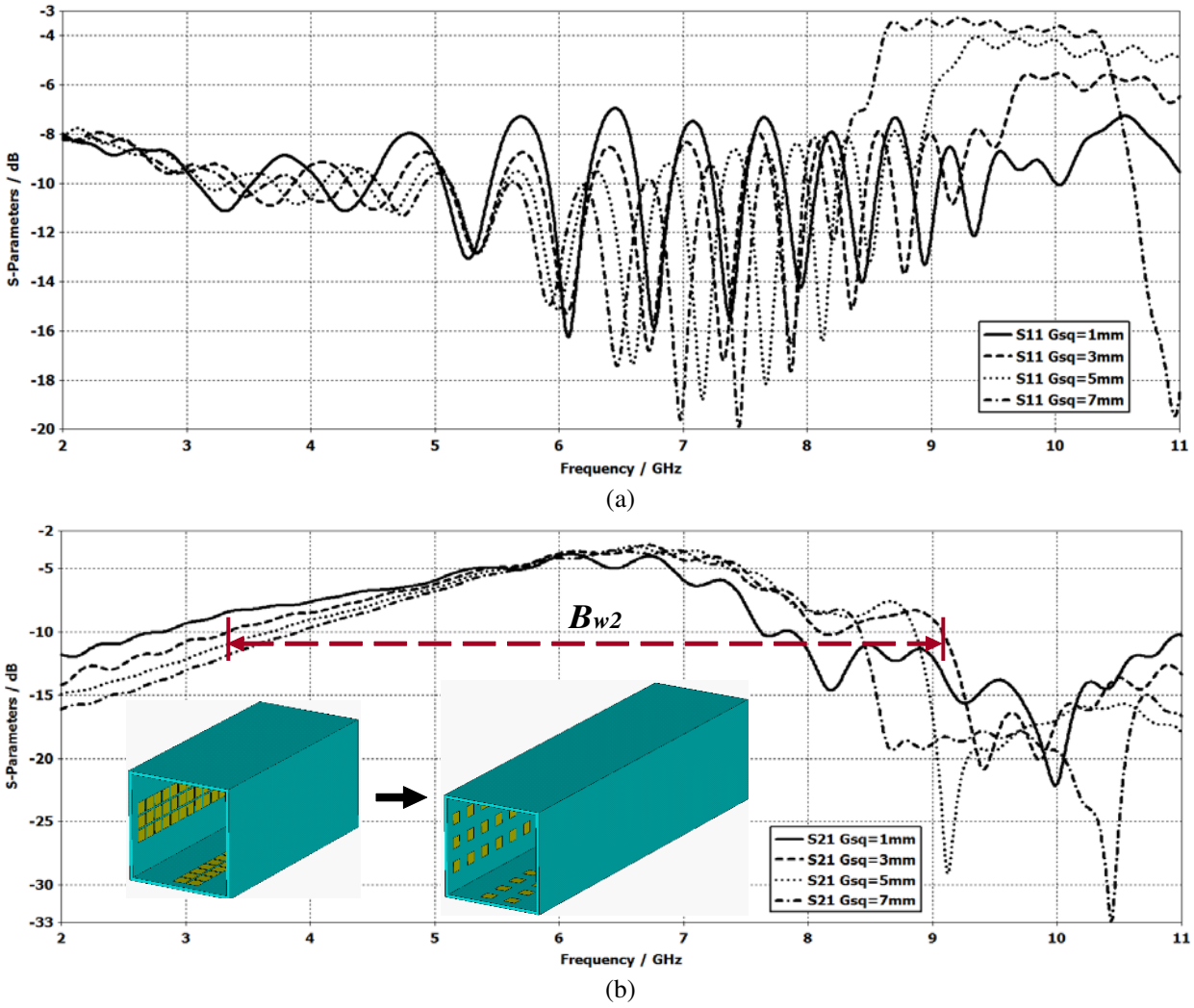

Figure 7. Simulated (a) S_{11} and (b) S_{21} for the parameter study on the inter space square element.

realized that higher reflection was obtained at higher frequencies from 8.5 GHz to 11 GHz when G_{sq} was increased. In the meantime, S_{21} presented less variation at frequencies below 6 GHz with different G_{sq}. The variation of G_{sq} affected and shifted S_{21} with the operating frequency band to higher and irregular frequencies. Overall, the optimized inter space square element was 3 mm with the widest B_{w2} from 3.4 GHz to 9 GHz.

3.3. Effect of Waveguide and DWS toward Monopole Antenna

Antenna parameters of return loss, gain and radiation pattern were measured at the Microwave Lab in Fakulti Kejuruteraan Elektronik & Kejuruteraan Komputer (FKEKK), Universiti Teknikal Malaysia Melaka (UTeM). Figure 8 shows the experimental setup to measure return loss, gain and radiation pattern. The return loss was measured by Vector Network Analyzer (VNA). Meanwhile, the measured gain was obtained by using the comparison method. Initially, horn antennas with known gain were located face-to-face at the transmitter and receiver sites to obtain the power received (P_1). Next, the Antenna Under Test (AUT) was placed at the receiver site to obtain power received (P_2). The gain of AUT could be obtained through the horn antenna with known gain at the receiver site and the magnitude difference between P_1 and P_2. Meanwhile, the radiation pattern measurement set the horn antenna and AUT at the transmitter and receiver sites, respectively with the azimuth angle *phi* equal

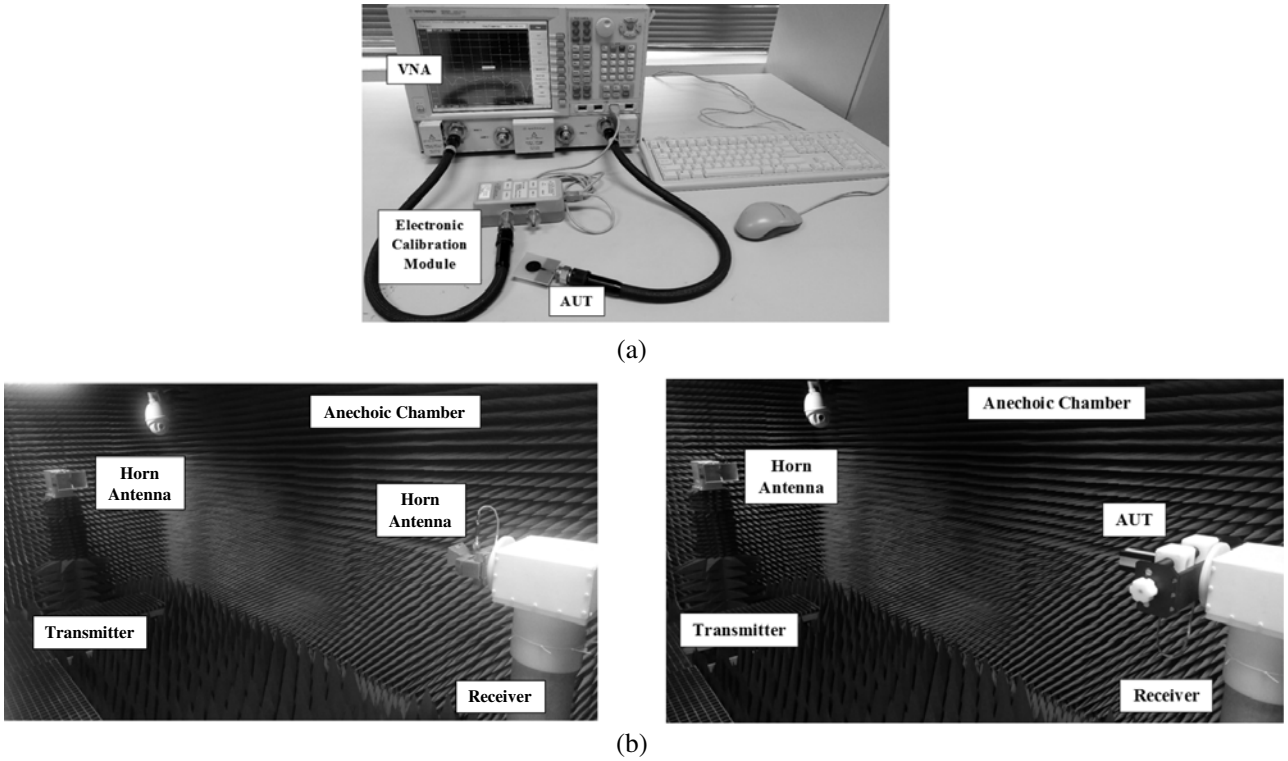

Figure 8. The experiment setup for (a) return loss, (b) gain and radiation pattern measurement.

to 0 and 90 degrees. The simulated results were validated by the measured ones.

The return loss (S_{11}) results are presented in Figure 9. Good agreement was noticed between simulated and measured S_{11} results. Initially, both Design A and Design B achieved wideband from 2.5 GHz to 11 GHz. With the integration of DWS, Design AD and Design BD maintained wideband characteristics of both Design A and Design B, whereas Design AC and Design BC showed multiband characteristics with narrower bandwidth. Design AC and Design BC achieved the widest bandwidth B_{w3} from 6 GHz to 11 GHz and B_{w4} from 8.5 GHz to 11 GHz, respectively at higher frequency range. Furthermore, the resonance frequencies (Marker 1–Marker 2) of Design A and Design B were shifted with the additional DWS. The shifted resonance frequencies of Design AD and Design BD were shown in Marker 3–Marker 4. Resonance frequency at higher frequency range was shifted the most with more than 0.5 GHz from Marker 2 to Marker 4 for both designs. Design A and Design B showed slightly different resonance frequencies at lower and higher frequency ranges. Design B demonstrated both resonance frequencies at a lower frequency range than Design A. Besides that, Design AC presented more fluctuated S_{11} results than Design BC. It was also realized that Design AC and Design BC demonstrated high reflection around 2 GHz–3 GHz due to f_c.

The measured gain was in agreement with the simulated one in Figure 10. Measured gain was lower than the simulated one due to fabrication errors, measurement alignment and distortion of environment during measurement. Overall, both Design A and Design B showed lower gains. Design AC enhanced its gain around 3 GHz–7 GHz in Region R_1. In the meantime, Design BC showed gain enhancement at frequency range of 3 GHz–5 GHz, 6.5 GHz–7.5 GHz and above 9.5 GHz in Regions R_3, R_4 and R_5, accordingly, whereas Design AC improved its gain in Regions R_1 and R_2 at a frequency range of 7.5 GHz–10 GHz. Design BD again presented gain improvement in Regions R_3, R_4 and R_5. For Design A, Design AD showed more significant gain improvement than Design AC with the magnitude differences d_1 and d_2 found in Regions R_1 and R_2 with the maximum magnitude difference d_2 of 2 dB at a frequency of 8.5 GHz. Design B showed a different scenario compared to Design A. Design BC showed significant gain improvement compared to Design BD with magnitude differences d_3 and d_4 in Regions R_3 and R_4. At a frequency of 4.5 GHz, more than 2 dB of gain was enhanced by Design BC for d_3.

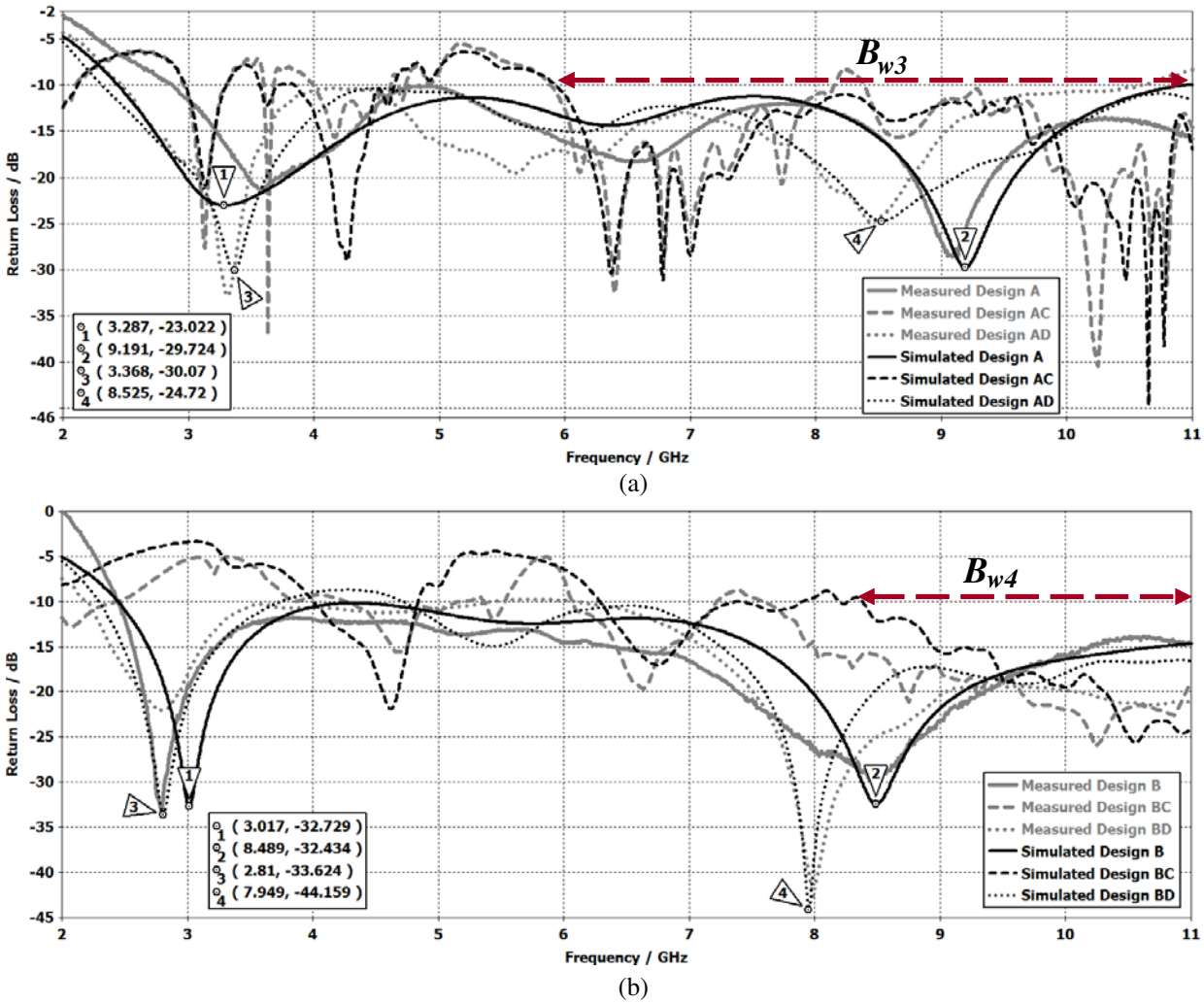

Figure 9. Simulated and measured S_{11} for (a) Design A and (b) Design B with waveguide and DWS.

With the wideband characteristics as shown earlier, both Design A and Design B demonstrated the highest efficiency overall in Figure 11. Both Design AD and Design BD still performed similarly, but there was a slightly lower efficiency than Design A and Design B. Design AC and Design BC showed very low efficiency at lower frequency range below 7 GHz as illustrated in Region R_6. Design AC showed higher efficiency than Design BC with magnitude difference d_5, d_6 and d_7 at frequencies 4 GHz, 5.5 GHz and 7.5 GHz, respectively. The maximum magnitude difference achieved more than 1.5 dB which was shown by d_6. At higher frequency of more than 8 GHz, all of Design B presented higher efficiency than all of Design A with the magnitude difference d_8 around 0.5 dB.

Figure 12 demonstrates the simulated directivity results. It was interesting to notice that all Design A and Design B with waveguide and DWS presented significant directivity improvement with 2 dBi–5 dBi in Region R_7 at lower frequencies below 6 GHz. Both Design A and Design B showed the lowest directivity overall. Design BC showed the maximum directivity improvement with the magnitude difference d_9 of almost 5 dBi at 4.5 GHz. Besides that, Design BC also showed improved directivity with the magnitude difference d_{11} of 2 dBi at frequency 7 GHz. Meanwhile, both Design AC and Design AD showed directivity enhancement with the magnitude difference d_{10} of 4 dBi at 4.5 GHz. Unlike Design BD, Design AD showed significant directivity improvement with the magnitude difference d_{12} of 2 dBi at a higher frequency of 8.5 GHz.

The simulated and measured radiation patterns are also plotted in Figure 13 for Design A and Design B at different resonance frequencies. Referring to Figure 13, the resonance frequencies of Design

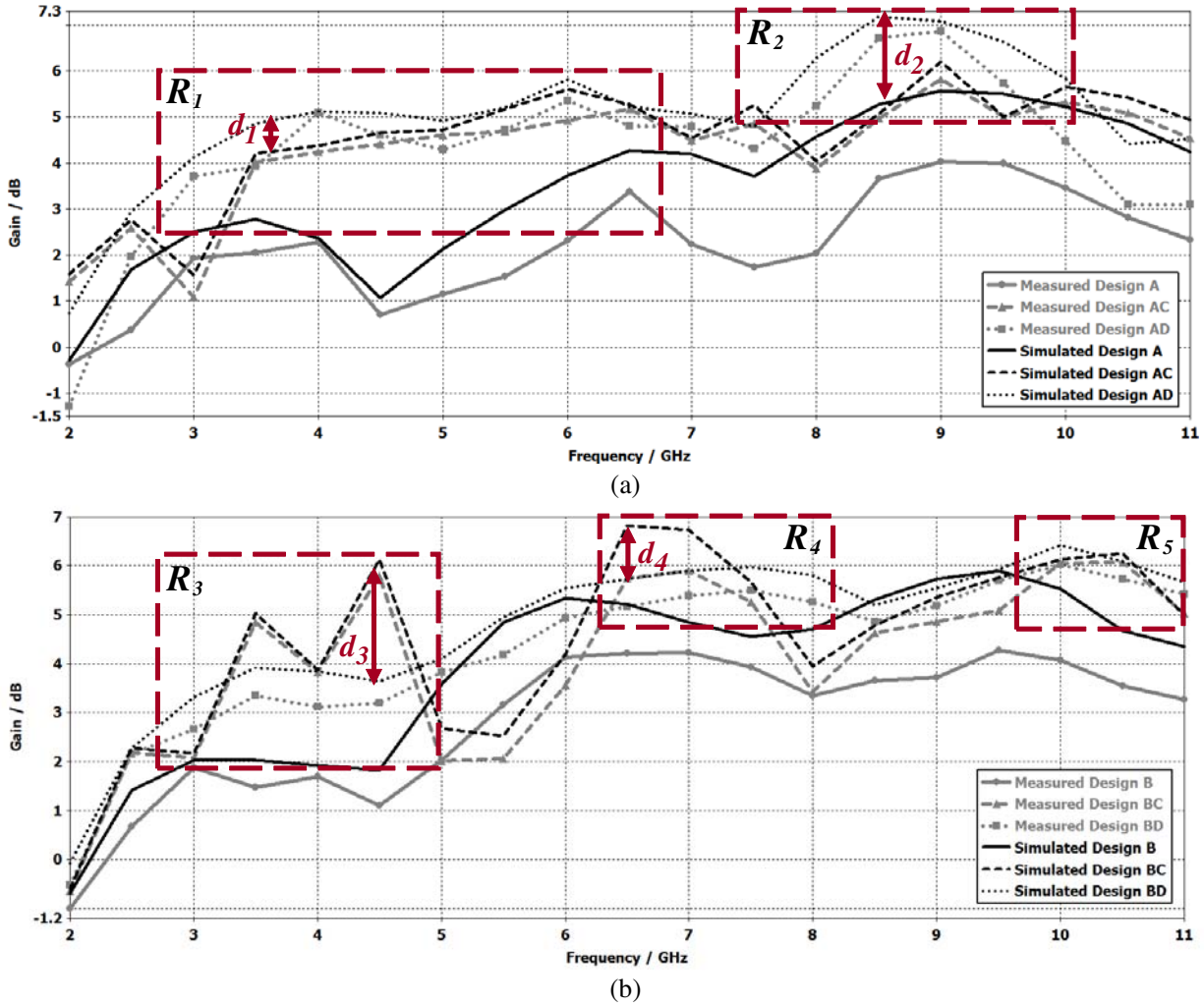

Figure 10. Simulated and measured gains for (a) Design A and (b) Design B with waveguide and DWS.

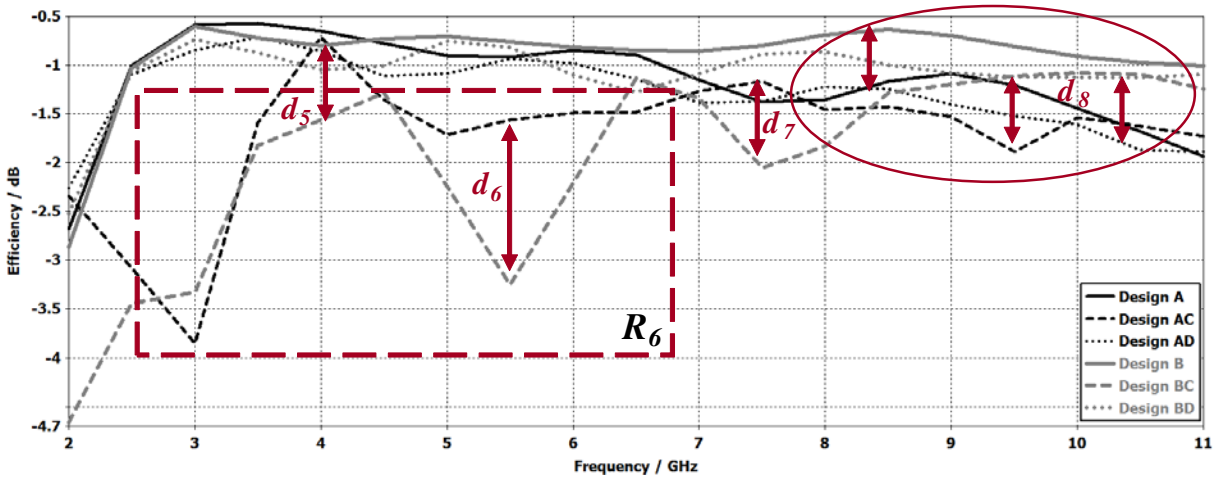

Figure 11. Simulated efficiency for Design A and Design B with waveguide and DWS.

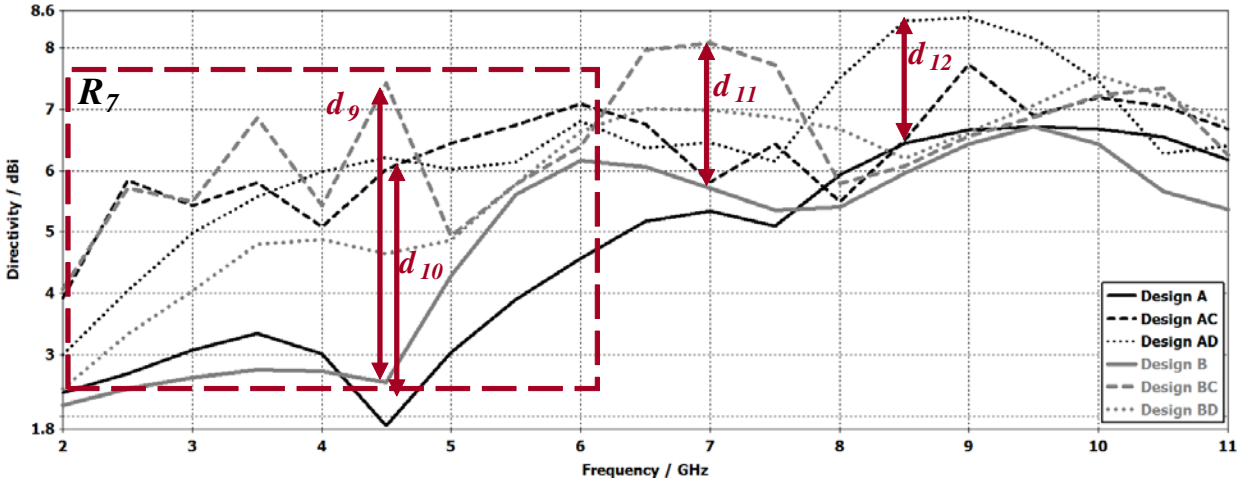

Figure 12. Simulated directivity for Design A and Design B with waveguide and DWS.

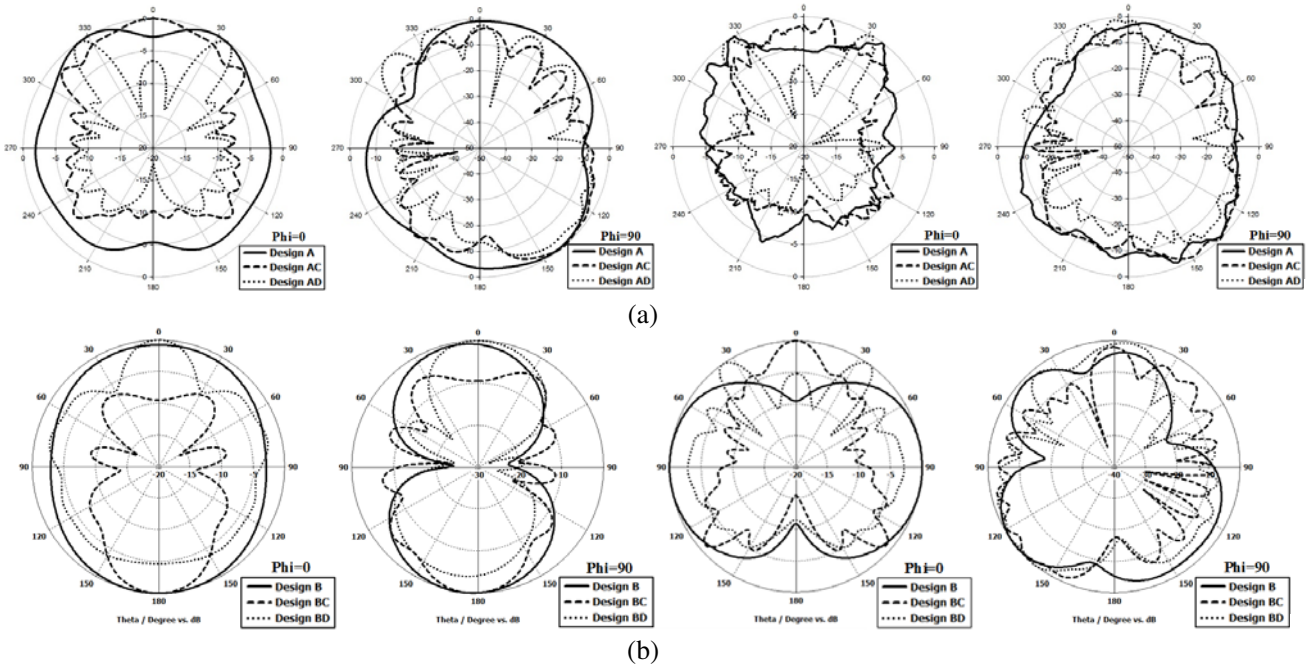

Figure 13. Simulated and measured radiation pattern for (a) Design A at 9 GHz and (b) Design B at 8.5 GHz.

A and Design B at a higher frequency range were 9 GHz and 8.5 GHz, accordingly. The angle was varied by 360 degrees at *theta* and *phi* and varied at 0 and 90 degrees. Compared to the simulated radiation pattern, the measured radiation pattern showed smaller beam and distortion with many minor lobes. For *phi* of 0 degree, a more obvious difference of radiation pattern was shown for both Design A and Design B with the addition of waveguide and DWS. Two major lobes were shown by both Design A and Design B at the 90 and 270 degrees. Meanwhile, Design AC and Design BC presented smaller beam with many minor lobes. Design AC showed major lobes direction at 0 degree. Design AD and Design BD demonstrated two major lobes directions at around 30 and 330 degrees in narrower beam for $phi = 0$ degree. Meanwhile, the radiation pattern for *phi* of 90 degrees showed a less significant variation. Design AC, Design AD, Design BC and Design BD showed almost similar radiation patterns to Design A and Design B with the number of minor lobes increased. Two major lobes with the major lobe direction of 120–150 degrees were shown in Design A and Design B for $phi = 90$ degrees.

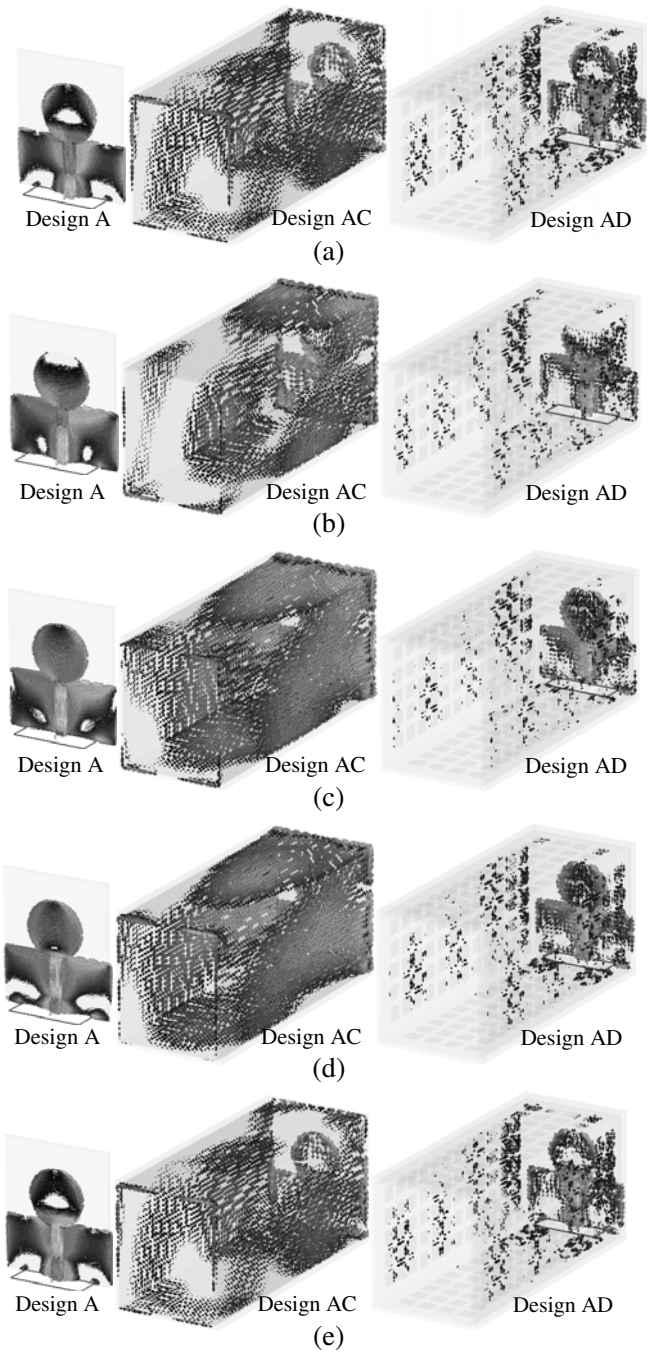

Figure 14. The surface current distribution of Design A with waveguide and DWS for five different phases of (a) 0, (b) 45, (c) 90, (d) 135 and (e) 180 degrees at frequency 4.5 GHz.

The surface current distribution is also plotted in Figure 14 to investigate the transmission through waveguide and DWS. The surface current distribution was shown for only Design A at frequencies higher than f_c, so that the wave was able to propagate through the waveguide. The surface current distributions were demonstrated for the phases of 0, 45, 90, 135 and 180 degrees at frequency 4.5 GHz. At phases of 90 and 135 degrees, the highest surface current concentration was distributed through the waveguide with the highest concentration of surface current at the circular radiating patch of the monopole antenna. Meanwhile, there was less surface current concentration for the DWS design. Since

the waveguide with DWS was not covered in full by copper, there was a degradation of propagated wave throughout the transmission. However, a waveform could be observed at the surface of DWS walls. Furthermore, higher surface current concentration was noted at both sides of the walls compared to the top and bottom walls of the DWS design.

Overall, it was noticed that all the antenna parameters were related to each other. With higher efficiency, the antenna was able to radiate successfully with lower reflection coefficient. Thus, higher directivity and gain could also be achieved at a higher possibility. With the higher directivity, the directional radiation pattern could be obviously seen.

4. CONCLUSION

This paper presents the effects of square Defected Waveguide Structure (DWS) toward wideband monopole antennas. Two monopole antennas with microstrip and CPW feed lines were integrated in waveguide and DWS. Both monopole antennas showed a wide bandwidth of 8.5 GHz and high efficiency of more than −2 dB. However, the monopole antennas showed lower gain and directivity in a miniaturized size. Monopole antennas with waveguide presented narrower bandwidth from 6 GHz to 11 GHz but a significant directivity improvement of 5 dBi at a lower frequency 4.5 GHz. Monopole antenna with square DWS demonstrated high directivity and gain in a wide bandwidth of 8.5 GHz. Higher gain was improved at around 4 dB at frequency 4.5 GHz, and high efficiency of more than −2 dB was achieved. In the future, the square DWS designs can be replaced by other shapes for example circular and spiral.

ACKNOWLEDGMENT

The authors would like to thank Ministry of Higher Education (MOHE) and Universiti Teknikal Malaysia Melaka (UTeM) to support this research work under the grant PJP/2017/FKEKK/HI13/S01541.

REFERENCES

1. Nikolaou, S. and M. A. B. Abbasi, "Design and development of a compact UWB monopole antenna with easily controllable return loss," *IEEE Transactions on Antennas and Propagation*, Vol. 65, No. 4, 2063–2067, 2017.
2. Dashti Ardakani, M., J. Pourahmadazar, and S. O. Tatu, "A monopole antenna with notch-frequency function for UWB application," *XXXIInd General Assembly and Scientific Symposium of the International Union of Radio Science (URSI GASS)*, 1–4, Montreal, QC, 2017.
3. Singh, K., A. Siwach, and L. Kaur, "Advancement in designing of wideband horn antenna," *International Journal of Engineering Trends and Technology (IJETT)*, Vol. 4, No. 4, 719–722, 2013.
4. Mistry, K., et al., "Measurement, simulation and optimization of wideband log-periodic antennas," *XXXIInd General Assembly and Scientific Symposium of the International Union of Radio Science (URSI GASS)*, 1–4, Montreal, QC, 2017.
5. Feng, G., L. Chen, X. Wang, X. Xue, and X. Shi, "Broadband circularly polarized crossed Bowtie dipole antenna loaded with parasitic elements," *IEEE Antennas and Wireless Propagation Letters*, No. 99, 1–1, 2017.
6. Lai, J. Y., C. W. Hsu, K. W. Li, and C. J. Wang, "A wideband CPW-fed monopole antenna with linear and circular polarizations," *IEEE International Symposium on Antennas and Propagation & USNC/URSI National Radio Science Meeting*, 327–328, San Diego, CA, 2017.
7. Farhan, M., S. G. Dhende, and B. G. Hogade, "Printed monopole antenna array: A technique to improve directive gain," *International Conference on Electrical, Electronics, and Optimization Techniques (ICEEOT)*, 264–268, Chennai, 2016.
8. Patil, S., R. Gupta, and S. Kharche, "Gain improvement of lower UWB monopole antenna using FSS layer," *International Conference on Nascent Technologies in Engineering (ICNTE)*, 1–5, Navi Mumbai, 2017.

9. Meriche, M. A., H. Attia, A. Messai, and T. A. Denidni, "Gain improvement of a wideband monopole antenna with novel artificial magnetic conductor," *17th International Symposium on Antenna Technology and Applied Electromagnetics (ANTEM)*, 1–2, Montreal, QC, 2016.
10. Samad, M. A. and A. K. Hamid, "Miniaturization of waveguide antenna using square/circular arrays of SRR," *5th International Conference on Electronic Devices, Systems and Applications (ICEDSA)*, 1–4, Ras Al Khaimah, 2016.
11. Wahid, A. and A. Munir, "Design of 9 GHz dual-polarized rectangular waveguide antenna," *2nd International Conference on Wireless and Telematics (ICWT)*, 44–46, Yogyakarta, 2016.
12. Zou, T., B. Zhang, and Y. Fan, "Design of a 73 GHz waveguide bandpass filter," *IEEE 9th UK-Europe-China Workshop on Millimetre Waves and Terahertz Technologies (UCMMT)*, 219–221, Qingdao, 2016.
13. Fang, D., B. Zhang, and J. He, "A E-band E-plane type waveguide bandpass filter," *IEEE 9th UK-Europe-China Workshop on Millimetre Waves and Terahertz Technologies (UCMMT)*, 180–182, Qingdao, 2016.
14. Uyama, K., S. Nishimura, H. Deguchi, and M. Tsuji, "Transmission characteristics of CRLH rectangular waveguides constructed by the Cutoff Modes of TM and TE waves," *International Conference on Electromagnetics in Advanced Applications (ICEAA)*, 728–731, Cairns, QLD, 2016.
15. Fu, Y. and N. Yuan, "Reflection and transmission between rectangular waveguide and EBG based TEM waveguide," *Asia-Pacific Microwave Conference Proceedings*, Vol. 3, 2, 2016.
16. Wartak, M. S., K. L. Tsakmakidis, and O. Hess., "Introduction to metamaterials," *Physics in Canada*, Vol. 67, No. 1, 30–34, 2011.
17. Dalenjan, M. S., P. Rezaei, M. Akbari, S. Gupta, and A. R. Sebak, "Radiation properties enhancement of a microstrip antenna using a new UC-EBG structure," *17th International Symposium on Antenna Technology and Applied Electromagnetics (ANTEM)*, 1–2, Montreal, QC, 2016.
18. Lucena, F. A. C. S., C. P. N. Silva, T. L. Pedrosa, and M. T. de Melo, "Gain enhancement of dual-band antenna using square loop FSS," *IEEE International Symposium on Antennas and Propagation & USNC/URSI National Radio Science Meeting*, 2169–2170, San Diego, CA, 2017.
19. Chetouah, F., N. Bouzit, I. Messaoudene, S. Aidel, M. Belazzoug, and Y. B. Chaouche, "Miniaturized printed rectangular monopole antenna with a new DGS for WLAN applications," *International Symposium on Networks, Computers and Communications (ISNCC)*, 1–4, Marrakech, 2017.
20. Wang, Y., T. Jiang, and Y. Li, "Development of a microstrip-fed multi-band antenna by means of defected microstrip structures," *Progress In Electromagnetic Research Symposium (PIERS)*, 1986–1988, Shanghai, 2016.
21. Das, L., A. Sahoo, D. Konhar, and D. Mishra, "A planar monopole antenna with DGS for bandwidth enhancement and U-slot for band-notch characteristics," *IEEE Conference on Information & Communication Technologies*, 977–980, JeJu Island, 2016.
22. Chin, S. J., M. Z. A. Abd Aziz, and M. R. Ahmad, "Microstrip-fed circular disc monopole antenna with defected waveguide structure," *International Journal of Electrical and Computer Engineering (IJECE)*, Vol. 8, No. 1, 189–197, 2018.
23. Liang, J., L. Guo, C. C. Chiau, X. Chen, and C. G. Parini, "Study of CPW-fed circular disc monopole antenna for ultrawideband applications," *IEE Proceedings — Microwaves, Antennas and Propagation*, Vol. 152, No. 6, 520–526, 2005.
24. Chin, S. J., M. Z. A. Abd Aziz, and M. R. Ahmad, "Comparative analysis of different defected waveguide structures towards monopole antenna," *Progress in Electromagnetics Research Symposium-Fall (PIERS-FALL)* 1428–1436, 2017.
25. Kwaha, B. J., O. N. Inyang, and P. Amalu, "The circular microstrip patch antenna-design and implementation," *International Journal of Recent Research and Applied Studies (IJRRAS)*, Vol. 8, No. 1, 86–95, 2011.
26. Whyte, G. W. M., *Antennas for Wireless Sensor Network Applications*, Ph.D. diss., University of Glasgow, Scotland, 2008.